The measurement of anomalous neutron inelastic cross-sections at electronvolt energy transfers

2004 J. Phys.: Condens. Matter 16 4811

(http://iopscience.iop.org/0953-8984/16/28/005)

INSTITUTE OF PHYSICS PUBLISHING JOURNAL OF PHYSICS: CONDENSED MATTER

J. Phys.: Condens. Matter **16** (2004) 4811–4832 PII: S0953-8984(04)75763-X

The measurement of anomalous neutron inelastic cross-sections at electronvolt energy transfers

J Mayers[1] **and T Abdul-Redah**[2]

[1] ISIS Facility, Rutherford Appleton Laboratory, Chilton/Didcot OX11 0QX, UK
[2] Physics Laboratory, University of Kent at Canterbury, Canterbury, Kent CT2 7NR, UK

Received 3 February 2004
Published 2 July 2004
Online at stacks.iop.org/JPhysCM/16/4811
doi:10.1088/0953-8984/16/28/005

Abstract

It has been proposed that short-lived quantum entanglement of protons in condensed matter systems would result in anomalous inelastic scattering cross-sections at electronvolt energy transfers. This proposal seems to be confirmed by neutron measurements on the VESUVIO spectrometer at ISIS and by measurements using other techniques. However, there have been a number of published suggestions of ways in which the observed effects on VESUVIO could be introduced by assumptions used in the data analysis. In this paper it is shown using experimental data and Monte Carlo simulations that these suggestions cannot explain the observed cross-section anomalies. The other assumptions of the data analysis are also examined. It is shown that the assumption of a Gaussian peak shape for the neutron Compton profile can introduce significant errors into the determination of cross-section ratios, but also cannot explain the observed anomalies.

1. Introduction

The neutron scattering experiments discussed in this paper were motivated by the proposal of Chatzidimitriou-Dreismann [1], that if the time interval during which an incident particle may interact with the target system is comparable to the quantum decoherence time, anomalous inelastic scattering cross-sections would be observed. It was suggested that quantum entanglement would give different ratios of cross-sections to those calculated from the sample composition and standard theory. This proposal obtained initial experimental support from experiments on liquid H_2O–D_2O mixtures using Raman light-scattering [2] and eV neutron scattering [3], performed on the VESUVIO spectrometer at the ISIS pulsed neutron source. These measurements showed anomalous ratios of the hydrogen and deuterium cross-sections. Subsequent VESUVIO measurements have been performed by Karlsson *et al* on niobium and palladium hydrides and deuterides [4–6] and by Chatzidimitriou-Dreismann *et al* on polystyrene [7], benzene [8] and other systems [9, 10]. These measurements all

exhibited anomalous ratios of the proton and deuterium inelastic cross-sections. Recently Chatzidimitriou-Dreismann *et al* [11] compared neutron cross-section results obtained on the amorphous polymer 'Formvar' ($C_8H_{14}O_2$) with the results of electron–proton scattering from the same material. The two techniques showed the same anomalous ratio of H and C inelastic cross-sections as a function of momentum transfer, despite the very different experimental methods used in the two cases.

Chatzidimitriou-Dreismann *et al* [7, 12], Karlsson and Lovesey [13, 14] and Karlsson [15] have presented different theoretical treatments of this effect. Both treatments share the assumption that the observations are due to quantum effects, which exist over the timescales $\sim 10^{-15}$ s accessed by measurements using eV neutrons. However, these theoretical interpretations have been questioned by Cowley [16] and by Colognesi [17]. The accuracy of the experimental results has also been questioned. It has been argued by Blostein *et al* [18–21] that the way in which the instrument resolution function is incorporated into the data fitting routines introduces serious errors into the data analysis, and that this could account for the observed anomalies. It has also been stressed by Cowley that an accurate correction of the measured data for the variation of the incident neutron intensity with energy is necessary and it has been suggested that any errors in this correction could also account for the observed anomalies. In the present paper these two points are specifically addressed. It is shown using measured data and Monte Carlo simulations of data that neither can explain the anomalies observed. The other assumptions of the data analysis are also critically examined.

The outline of the paper is as follows. In section 2, the expression used to fit the VESUVIO data is derived. Section 3 describes the way in which the instrument resolution is incorporated into the data analysis. Section 4 describes the Monte Carlo (MC) procedure used to test the fitting programs. In sections 5–7 the influence of instrumental effects on the results are evaluated, using MC simulations and also by comparing data taken under different experimental conditions. Section 5 considers the effects of the correction for the incident beam intensity. Section 6 considers the systematic errors generated by approximations made to incorporate the instrument resolution in the fitting programs. Section 7 discusses effects dependent on sample size, such as attenuation, multiple scattering and detector dead time effects. Sections 8 and 9 discuss the validity of the assumptions (a) that scattering can be described within the impulse approximation (IA), and (b) that the atomic momentum distributions have Gaussian peak shapes. Section 10 contains a summary and conclusions.

2. Theory of the data analysis procedure

2.1. Count-rates in time of flight neutron scattering experiments

We first consider a system of N identical atoms, scattering neutrons into a detector subtending solid angle $\mathrm{d}\Omega$, at scattering angle θ. It follows from the definition [22] of the partial differential scattering cross-section $\mathrm{d}^2\sigma/\mathrm{d}\Omega\,\mathrm{d}E$, that the number of neutrons with incident energies in the range E_0 to $E_0 + \mathrm{d}E_0$, detected with final energies between E_1 and $E_1 + \mathrm{d}E_1$, is

$$C_{\mathrm{D}}(E_0, E_1)\,\mathrm{d}E_0\,\mathrm{d}E_1 = I(E_0)D(E_1)\frac{\mathrm{d}^2\sigma(E_0, E_1, \theta)}{\mathrm{d}\Omega\,\mathrm{d}E_1}\,\mathrm{d}\Omega\,\mathrm{d}E_0\,\mathrm{d}E_1 \tag{2.1}$$

where $I(E_0)\,\mathrm{d}E_0$ is the number of incident neutrons/unit area with energies between E_0 and $E_0 + \mathrm{d}E_0$, and $D(E_1)$ is the probability that a neutron of energy E_1 is detected. It follows from standard theory [22] that for isotropic scattering,

$$\frac{\mathrm{d}^2\sigma(E_0, E_1, \theta)}{\mathrm{d}\Omega\,\mathrm{d}E_1} = |b|^2\sqrt{\frac{E_1}{E_0}}S(q, \omega) \tag{2.2}$$

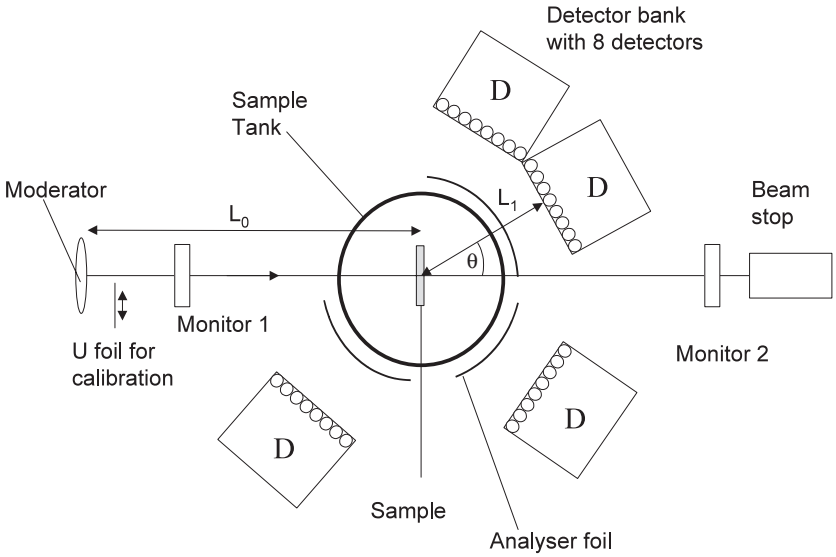

Figure 1. A schematic representation of the VESUVIO spectrometer at ISIS.

where b is the nuclear scattering length, the energy transfer in the measurements is

$$\omega = E_0 - E_1 \tag{2.3}$$

and the momentum transfer is

$$q = \sqrt{2m}\left(E_0 + E_1 - 2\sqrt{E_0 E_1}\cos\theta\right)^{1/2}. \tag{2.4}$$

The velocity of the scattered neutron is

$$v_1 = \sqrt{2E_1/m} \tag{2.5}$$

with a similar expression for the velocity v_0 of the incident neutron, where m is the neutron mass. The neutron time of flight t is thus

$$t = \frac{L_0}{v_0} + \frac{L_1}{v_1} \tag{2.6}$$

where L_0 is the incident flight path and L_1 is the final flight path (see figure 1). Equations (2.5) and (2.6) can be used to define E_0 in terms of E_1 and t.

$$E_0(E_1, t) = \frac{m}{2}\left(\frac{L_0 v_1}{v_1 t - L_1}\right)^2 \tag{2.7}$$

and the total number of neutrons detected in a time channel between t and $t + \mathrm{d}t$ can be expressed as

$$C(t)\,\mathrm{d}t = \left[\int C_{\mathrm{D}}[E_0(t, E_1), E_1]\frac{\mathrm{d}E_0(t, E_1)}{\mathrm{d}t}\,\mathrm{d}E_1\right]\mathrm{d}t. \tag{2.8}$$

An alternative and equally valid approach, used by Blostein *et al* [18], is to calculate $C(t)$ by expressing E_1 as a function of t and E_0 and integrating over E_0. However, it is more convenient to use equation (2.8) when discussing an 'inverse geometry' instrument such as VESUVIO, where the energy of the scattered neutron is analysed. It follows from (2.5) and (2.7) that

$$\frac{\mathrm{d}E_0}{\mathrm{d}t} = \left(-\frac{2^{3/2}}{L_0 m^{1/2}}\right)E_0^{3/2}. \tag{2.9}$$

For an ideal inverse geometry instrument, in which L_0, L_1, θ are precisely known and only neutrons of a precisely defined energy E_R are detected, i.e.

$$D(E_1) = D(E_R)\delta(E_1 - E_R). \tag{2.10}$$

It follows from (2.1) and (2.8)–(2.10) that

$$C(t) = 2\left(\frac{2}{m}\right)^{1/2} \frac{E_0^{3/2}}{L_0} I(E_0) D(E_R) N \frac{d^2\sigma}{d\Omega\, dE_1}\, d\Omega \tag{2.11}$$

where $E_0(E_R, t)$ is defined via (2.7). Equation (2.11) is the standard expression for the count rate in an inverse geometry time of flight spectrometer [23].

2.2. The impulse approximation

The VESUVIO spectrometer is mainly used to determine atomic momentum distributions in condensed matter systems, by 'deep inelastic neutron scattering' (DINS). DINS relies upon the fact that at sufficiently high momentum transfer, the impulse approximation (IA) can be used to interpret data. The validity of the IA in neutron scattering has been discussed by many authors [24–27] and at the energy and momentum transfers attained on VESUVIO is accurate to within ∼5% in hydrogenous samples [28]. A basic assumption of the IA is that for neutron wavelengths much less than the interatomic spacing, atoms scatter incoherently. Thus if atoms of different mass M are present in the sample, it follows from (2.11) that the count rate is

$$C(t) = 2\left(\frac{2}{m}\right)^{1/2} \frac{E_0^{3/2}}{L_0} I(E_0) D(E_R) \sum_M N_M \frac{d^2\sigma_M}{d\Omega\, dE_1}\, d\Omega \tag{2.12}$$

where N_M is the number of atoms of mass M and $d^2\sigma_M/d\Omega\, dE_1$ is the partial differential cross-section for mass M. The IA effectively treats the scattering as single atom 'billiard ball' scattering with conservation of momentum and kinetic energy of the neutron + target atom. The dynamic structure factor for atoms of mass M is thus [22]

$$S_M(\vec{q}, \omega) = \int n_M(\vec{p})\delta\left(\omega + \frac{p^2}{2M} - \frac{(\vec{p} + \vec{q})^2}{2M}\right) d\vec{p} \tag{2.13}$$

where $n_M(\vec{p})$ is the atomic momentum distribution for mass M. It is important to understand that the total scattering cross-section given by the IA is the 'free atom' value, which is not the same as the cross-section in the neutron–nucleus centre of mass frame. If

$$n_M(\vec{p}) = \delta(\vec{p}) \tag{2.14}$$

it follows from (2.13) and (2.2) that

$$\frac{d^2\sigma_M}{d\Omega\, dE_1} = b_M^2 \sqrt{\frac{E_1}{E_0}}\delta\left(\omega - \frac{q^2}{2M}\right) \tag{2.15}$$

where b_M is the 'bound' scattering length for atoms of mass M. Integrating equation (2.15) over the solid angle $d\Omega$ and final energies E_1 gives [22] the 'free atom' cross-section.

$$\int \frac{d^2\sigma_M}{d\Omega\, dE_1}\, dE_1\, d\Omega = \frac{4\pi b_M^2}{(1 + M/m)^2} = \frac{\sigma_M^2}{(1 + M/m)^2} \tag{2.16}$$

where σ_M is the standard tabulated 'bound' total scattering cross-section for mass M.

It follows from (2.13) that

$$S_M(q, \omega) = \frac{M}{q} J_M(y_M) \tag{2.17}$$

where

$$y_M = \frac{M}{q}\left(\omega - \frac{q^2}{2M}\right). \tag{2.18}$$

and

$$J_M(y_M) = \int n_M(\vec{p})\delta(y_M - \vec{p}\cdot\vec{q}/q)\,\mathrm{d}\vec{p}. \tag{2.19}$$

The 'neutron Compton profile' $J_M(y_M)$ is the probability distribution of the momentum component of mass M along the direction of $\vec{q}$ and is analogous to the 'Compton profile', measured in Compton scattering of photons from electrons.

It follows from equations (2.17) and (2.2) that

$$\frac{\mathrm{d}^2\sigma_M}{\mathrm{d}\Omega\,\mathrm{d}E_1} = b_M^2\sqrt{\frac{E_1}{E_0}}\frac{M}{q}J_M(y_M). \tag{2.20}$$

Combining equations (2.12) and (2.20)

$$C(t) = \frac{E_0 I(E_0)}{q}\sum_M A_M M J_M(y_M) \tag{2.21}$$

where

$$A_M = \frac{2}{L_0}D(E_\mathrm{R})\sqrt{\frac{2E_\mathrm{R}}{m}}\Delta\Omega N_M b_M^2 \tag{2.22}$$

is proportional to the scattering intensity from mass M.

2.3. Fitting expression

In the derivation of equation (2.21) it is assumed that the 'instrument parameters' L_0, L_1, θ and E_1 are known exactly. In reality these quantities can be determined only according to some probability distribution $P(L_0, L_1, \theta, E_1)$, which determines the instrument resolution. The measured count rate $C_\mathrm{m}(t)$ is an average over the possible values of these parameters, weighted by their probability of occurrence

$$C_\mathrm{m}(t) = \int C(t)P(L_0, L_1, \theta, E_1)\,\mathrm{d}L_0\,\mathrm{d}L_1\,\mathrm{d}\theta\,\mathrm{d}E_1. \tag{2.23}$$

Thus the exact incorporation of the instrument resolution function would entail the evaluation of this four dimensional integral for each data point, in addition to the convolution in t, required to incorporate the uncertainty in the measurement of time of flight. To reduce data processing times, the approximation is made in the data analysis that the resolution can be incorporated as a single convolution in t space, with a different resolution function $R_M(t)$ for each mass. Thus (2.21) is modified to

$$C_\mathrm{m}(t) = \left[\frac{E_0 I(E_0)}{q}\right]\sum_M A_M M J_M(y_M) \otimes R_M(t). \tag{2.24}$$

The approximation of replacing the exact expression (2.23) by (2.24) is referred to in the rest of the paper as the 'convolution approximation' (CA).

A second approximation of the data analysis is that $J_M(y_M)$ is assumed to have a normalized Gaussian form

$$J_M(y_M) = \frac{1}{\sqrt{2\pi w_M^2}}\exp\left(\frac{-y_M^2}{2w_M^2}\right). \tag{2.25}$$

The data analysis consists of fitting equations (2.24) and (2.25) to the data with two fitting parameters for each atomic mass, A_M and w_M. A_M determines the integrated peak intensity corresponding to a mass M, and w_M determines the peak width. It follows from (2.22) that

$$\frac{A_M}{A_{M'}} = \frac{N_M b_M^2}{N_{M'} b_{M'}^2} = \frac{N_M \sigma_M}{N_{M'} \sigma_{M'}} \tag{2.26}$$

where σ_M is the 'bound' cross-section for mass M and $\sigma_{M'}$ that for mass M'. Thus if the sample composition (and hence $N_M/N_{M'}$) is known, the ratios of cross-sections for atoms of different masses can be determined from the ratio of the fitted parameters A_M and $A_{M'}$. All results discussed in this paper were obtained in this way.

There are a number of possible sources of error in the determination of cross-section ratios from the fitting expression defined by (2.24) and (2.25), which will be examined in this paper.

(1) The incident spectrum intensity $I(E_0)$ must be accurately known.
(2) The incorporation of the resolution function components as Gaussian or Lorentzian functions is an approximation. Furthermore, incorporation of the resolution function as a convolution in t is an approximation.
(3) Multiple scattering and sample attenuation effects may change the fitted cross-section ratios.
(4) An implicit assumption in equations (2.21)–(2.23) is that the probability $D(E_1)$ that a neutron of energy E_1 is detected is independent of t, which is not true if detector dead time effects are significant.
(5) The impulse approximation is strictly valid only as $q \to \infty$, and corrections at the finite q of measurements must therefore be evaluated.
(6) The functions $J_M(y_M)$ may have non-Gaussian peak shapes.

3. The VESUVIO resolution function

It is assumed in the data analysis that the distributions of instrument parameters L_0, L_1, θ and E_1 are statistically independent, and that these distributions can be defined in terms of mean values, $\bar{L}_0$, $\bar{L}_1$, $\bar{\theta}$, $\bar{E}_1$ and widths of the distributions, ΔL_0, ΔL_1, $\Delta\theta$, ΔE_1. Both mean values and widths are determined by calibration measurements, as described previously [29]. For the calculation of E_0, q, y_M in terms of t, in the fitting expression (2.24), the mean values $\bar{L}_0$, $\bar{L}_1$, $\bar{\theta}$ and $\bar{E}_1$ are used. The widths are used to determine the mass dependent resolution widths of the functions $R_M(t)$ as follows.

For a given M, the position $t_M(L_0, L_1, \theta, E_1)$ of the peak centre in time of flight is determined by equation (2.6) and the relation

$$\frac{v_1}{v_0} = \frac{\cos\theta + \sqrt{(M/m)^2 - \sin^2\theta}}{M/m + 1}. \tag{3.1}$$

Equation (3.1) follows from the assumption of the IA that the peak centre corresponds to scattering from an atom with zero momentum, with conservation of momentum and kinetic energy. The width in t due to the uncertainty in for example E_1 is calculated as

$$\Delta t_{ME_1} = \frac{\partial t_M}{\partial E_1} \Delta E_1 \tag{3.2}$$

with similar expressions for the other resolution components in L_0, L_1 and θ. All resolution components other than the energy resolution are assumed to have a Gaussian peak shape in t and their widths are therefore added in quadrature.

$$\Delta t_{MI}^2 = \left(\frac{\partial t_M}{\partial L_0}\Delta L_0\right)^2 + \left(\frac{\partial t_M}{\partial L_1}\Delta L_1\right)^2 + \left(\frac{\partial t_M}{\partial \theta}\Delta\theta\right)^2. \tag{3.3}$$

The resolution function for these components is represented as a Gaussian in t, with standard deviation Δt_{MI}.

On VESUVIO the final energy is determined using the filter difference method [30], where two measurements are taken, one with an absorbing filter placed between the sample and detector and one with the filter removed. The difference between these two measurements is determined by the probability that the filter absorbs a neutron. This is

$$A(E_1) = 1 - \exp[-Nd\sigma(E_1)] \tag{3.4}$$

where N is the number of filter atoms cm^{-3}, the filter thickness is d and the filter total cross-section is $\sigma(E_1)$. The effective detection probability $D(E_1)$ is equal to the product of the filter absorption with the detector efficiency $\eta(E_1)$.

$$D(E_1) = A(E_1)\eta(E_1). \tag{3.5}$$

Filters with resonance absorption peaks, which absorb neutrons only in a narrow range of energies, are used to determine E_1. Two filters have been used in the measurements, either an Au filter with $Nd = 7.35 \times 10^{19}$ cm^{-2}, which defines a final energy $E_1 = 4908$ meV, with an approximately Lorentzian shape of half width at half maximum (HWHM) $\Delta E_1 \sim 140$ meV, or a U filter with $Nd = 1.46 \times 10^{20}$ cm^{-2}, $E_1 = 6671$ and an approximately Gaussian shape with standard deviation $\Delta E_1 \sim 63$ meV. For the Au filter, the total resolution function $R_M(t)$ is therefore represented as a convolution of a Lorentzian of HWHM Δt_{ME_1} and a Gaussian of standard deviation Δt_{MI}, whereas with the U filter analyser $R_M(t)$ is represented as a Gaussian function of standard deviation $\sqrt{\Delta t_{ME_1}^2 + \Delta t_{MI}^2}$.

4. Monte Carlo simulations of VESUVIO

Monte Carlo (MC) simulations of VESUVIO data can be performed using the computer code DINSMS, which has been described previously [31]. The MC program follows individual neutron histories through the spectrometer and then bins them in t, according to the time they have taken to travel between moderator and detector. The input to the program is

(1) The mean flight paths $\bar{L}_0$, $\bar{L}_1$ and the scattering angle $\bar{\theta}$ for each detector, defined by the position of the sample and detector centres.
(2) The incident neutron spectrum intensity $I(E_0)$, the moderator size and the probability distribution of times the neutron leaves the moderator.
(3) Definition of the sample in terms of
   (a) the sample size, geometry and composition N_M.
   (b) $\mathrm{d}^2\sigma_M/\mathrm{d}\Omega\,\mathrm{d}E_1$ for each mass. This is defined by equations (2.19) and (2.20), and input values of σ_M and $J_M(y_M)$.
(4) The detector size, geometry and efficiency $\eta(E_1)$, calculated from the known thickness and doping levels of the ^{6}Li doped glass scintillator detectors used on VESUVIO.
(5) The filter absorption $A(E_1)$. This is calculated from the known filter thickness and the tabulated neutron resonance parameters for the Au and U resonances [32]. All final energies between 0.1 and 60 eV are included in the definition of the filter resolution, for both Au and U filters.

DINSMS exactly incorporates resolution effects, multiple scattering and sample attenuation and is used in this paper to assess systematic errors introduced into cross-section ratios, derived by fitting data with equation (2.24).

The procedure followed is

(a) Simulate a lead calibration measurement and use the standard instrument calibration routines [29] to determine the energy width ΔE_1 for each detector.
(b) Generate simulated data sets for the sample and use the standard instrument fitting routines, incorporating equations (2.24) and (2.25) and the fitted value of ΔE_1 from step (a), to determine the cross-section ratios.
(c) Compare the fitted cross-section ratios $\sigma_M/\sigma_{M'}$ with those input to the MC simulation.

Data are simulated for all detectors used in measurements and the simulated data are analysed in precisely the same way as real data. Simulations with 'perfect resolution' can also be made by setting the moderator, sample and detector sizes to $\sim 10^{-6}$ cm and all final energies to exactly 4.908 eV, so that L_0, L_1, θ and E_1 are precisely defined.

5. Correction for incident neutron intensity

5.1. Determination of $I(E_0)$

It has been stressed [16, 18–20] that an accurate determination of the incident neutron intensity $I(E_0)$ is essential for the determination of cross-section ratios on VESUVIO. $I(E_0)$ was measured using the VESUVIO incident beam monitor 1 (see figure 1). The incident energy of the neutrons is related to their time of flight measured in the monitor via

$$E_0(t) = \tfrac{1}{2}m(L/t)^2. \tag{5.1}$$

The incident beam intensity is related to the measured monitor counts $C_{\mathrm{m}}(t)\,\mathrm{d}t$ via

$$I(E_0)\,\mathrm{d}E_0 = \frac{C_{\mathrm{m}}(t)}{\eta_{\mathrm{m}}(E_0)}\,\frac{\mathrm{d}t}{\mathrm{d}E_0}\,\mathrm{d}E_0 \tag{5.2}$$

where $\eta_{\mathrm{m}}(E_0)$ is the monitor efficiency at energy E_0. An example of a measurement of $I(E_0)$, determined from (5.2), is shown in figure 2(a), together with a fit to the function

$$I(E_0) = B/E^{\gamma} \tag{5.3}$$

with B and γ as adjustable parameters. The fit gave $\gamma = 0.90$ with statistical errors at the $\sim 10^{-5}$ level, in agreement with Monte Carlo calculations of the moderator performance [33], which predict that $\gamma = 0.9$. A large number of such data sets, collected over the past 10 years, all give consistent values $\gamma = 0.90 \pm 0.01$.

As a further test on the accuracy of the measurement of $I(E_0)$, a second procedure was used to determine γ. A U filter was cycled in the incident beam (see figure 1) and the difference between the counts with the foil in and foil out was calculated. An example of such a difference measurement is shown in figure 2(b). The difference foil out − foil in is given by

$$\Delta(t)\,\mathrm{d}t = I(E_0)\,\frac{\mathrm{d}E_0}{\mathrm{d}t}\,\mathrm{d}t\,\eta_{\mathrm{m}}(E_0)A(E_0) \tag{5.4}$$

where $A(E_0)$ is the filter absorption, defined in equation (3.4). It follows from (5.4) that the sum of counts in time of flight, over the area of a single resonance peak, centred at E_{R}, is

$$\int_{t_1}^{t_2} \Delta(t)\,\mathrm{d}t = \int I(E_0)\eta_{\mathrm{m}}(E_0)A(E_0)\,\mathrm{d}E_0 \approx I(E_{\mathrm{R}})\eta_{\mathrm{m}}(E_{\mathrm{R}})\alpha_{\mathrm{R}} \tag{5.5}$$

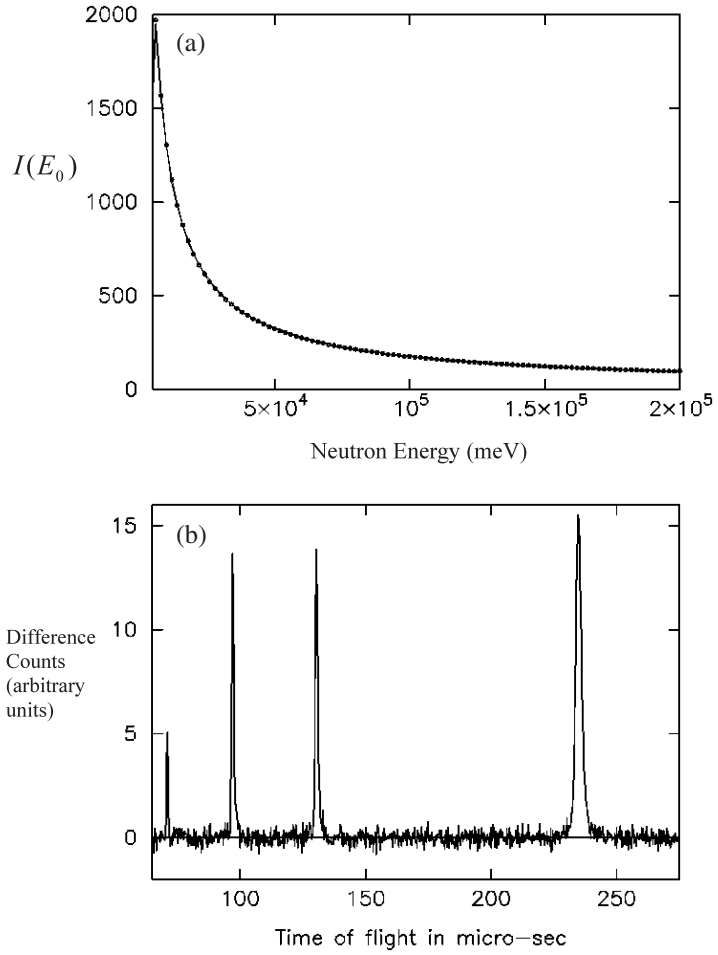

Figure 2. (a) The points are the incident neutron spectrum after correction for the monitor efficiency. The solid curve is a fit to equation (5.3). (b) Difference between monitor spectra obtained with a U foil in the incident beam and with no foil in the beam. The four peaks correspond to resonances at 6.7, 22, 37 and 66 eV.

where t_1 and t_2 are chosen to include only a single resonance peak and

$$\alpha_R = \int A(E_0)\,\mathrm{d}E_0 \tag{5.6}$$

is the total absorption corresponding to the resonance peak chosen. $I(E_0)$ and $\eta(E_0)$ can be taken outside the integral in (5.5) due to the narrowness of the peaks. The absorption factor α_R was also calculated from (3.4) and (5.6) for U resonances at 6.7, 21, 37 and 66 eV, using tabulated resonance parameters for U [32], which are known with very high accuracy. The quantity Nd was determined by weighing the filter, which has uniform thickness over a 10 cm × 10 cm area. The detector efficiency $\eta_m(E_R)$ can also be calculated, and for the 0.5 mm thick glass beads used in standard ISIS monitors is $\propto 1/\sqrt{E_R}$ to ∼1%. Using calculated values of α_R and $\eta_m(E_R)$, $I(E_R)$ was calculated from S_R for each of the four resonance peaks. These values of $I(E_R)$ were then fitted to the function $I(E_0)$ defined in equation (5.3), to obtain γ. The advantage of this measurement over the direct determination of γ from the full monitor

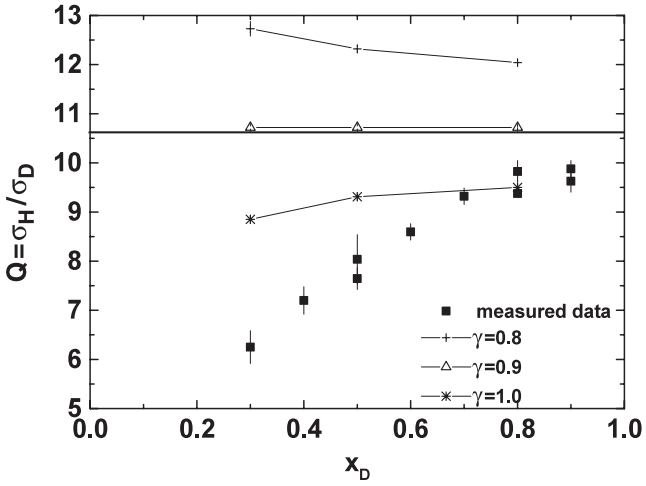

Figure 3. The points ++ were obtained from fits to simulations for H_2O/D_2O mixtures with $\gamma = 0.8$, the points $\Delta\Delta$ were for $\gamma = 0.9$ and $**\gamma = 1.0$. The points ■■ show the results from VESUVIO data collected using an Au filter.

Table 1. Measurements of γ obtained by the methods described in section 5. The means with standard deviations are also given.

Run	U foil transmission	Direct measurement
10 539	0.93	0.89
10 540	0.90	0.89
10 541	0.94	0.89
10 545	0.90	0.89
10 550	0.96	0.90
Mean	0.93 ± 0.01	0.892 ± 0.02

spectra is that γ is determined only by the neutrons absorbed by the foil. Thus, for example, any delayed neutron background has little effect on γ values obtained in this way. The results obtained are shown in column 2 of table 1. For comparison, values of γ obtained by direct fitting of the spectra as in figure 2(a) are also given. There is a small systematic difference in γ values obtained by the two different methods, but, as will be shown in the following section, this difference is much too small to explain the anomalies observed.

5.2. Effects of errors in $I(E_0)$

The measurements described in [3] were of the ratio of the H and D cross-sections, σ_H/σ_D, in mixtures of D_2O and H_2O as a function of D_2O concentration x_D. In order to test how sensitive these measurements are to the accuracy with which γ is known, complete data sets were simulated by DINSMS, as described in section 4, using perfect resolution. Incident intensities of the form in (5.3), with $\gamma = 0.8, 0.9$ and 1.0, were input to three different simulations. These three simulations were then fitted using the standard data analysis routines, which assume $\gamma = 0.9$. Values of σ_H/σ_D were calculated from the fitted parameters, as an average over the angular range 50°–75°, following exactly the same procedure used for real data. Figure 3 shows values of σ_H/σ_D as a function of x_D, obtained from for the three different values of γ input to the simulation. Also shown are the data measured in [3]. With an input value to

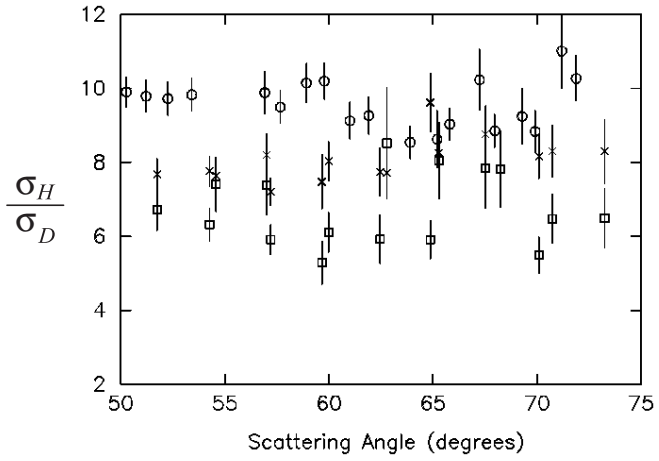

Figure 4. Values of σ_H/σ_D obtained from fitting individual time of flight spectra for the H_2O/D_2O data published in [3] as a function of scattering angle. The points ∘∘ were for $x_D = 0.9$, ×× for $x_D = 0.5$ and for $x_D = 0.3$. Within error at a given x_D, there is no angular dependence.

DINSMS of $\gamma = 0.9$, the fitted parameters were identical within statistical error to the values input to the simulation. As γ increases above this value, the values of σ_H/σ_D obtained from the fit decrease, but it is clear from figure 3 that γ would have to be ∼1.1 to account for the large anomalies observed in the data. Similar comments apply to anomalies observed in other systems. This is well outside the errors in the measurement of γ given in table 1.

5.3. Jacobians

Cowley [16] has also pointed out that there is a large Jacobian factor involved in any conversion between a VESUVIO time of flight scan in q, ω space and a constant q scan, and suggested that any errors in the incorporation of this factor could seriously affect the peak areas obtained from the fitting. However, we note that the only Jacobian, dE_0/dt, involved in the fitting expression is well known [23]. Furthermore, neglecting resolution effects, if the IA is valid, equation (2.21) is an *exact* expression for the count rate as a function of t and is true for any point in q, ω space accessed by the spectrometer. Thus the exact line of the scan in q, ω space is immaterial, since in principle every scan will give the same values for the fitting parameters, whether it is at constant $\vec{q}$ or constant θ. For example, fitting DINSMS simulations with perfect resolution to equation (2.21) recovers the cross-section ratios input to the simulation to within a statistical error ∼1%, at any scattering angle, as can be seen in the $\gamma = 0.9$ simulation shown in figure 3.

It should also be noted that any errors in either the assumed Jacobian dE_0/dt, or $I(E_0)$, would produce a consistent angular dependence in the cross-section ratios of H to heavier atoms in all samples, which is not observed. The ratio σ_H/σ_D obtained from measurements on H_2O/D_2O mixtures is essentially independent of angle. This is illustrated in figure 4, where this ratio is shown as a function of angle for three different values of D_2O concentration x_D, measured in [3]. VESUVIO measurements on NbD [4] and polystyrene [5] also show ratios of H to heavier atom cross-sections which are independent of angle. In contrast, measurements on Formvar [11], shown in figure 5, give a marked fall off in the H to heavy atom cross-section ratio as the scattering angle, and hence q is increased. Measurements on NbH [4] have an even stronger angular dependence. Thus no single γ value can explain the anomalies observed in different samples.

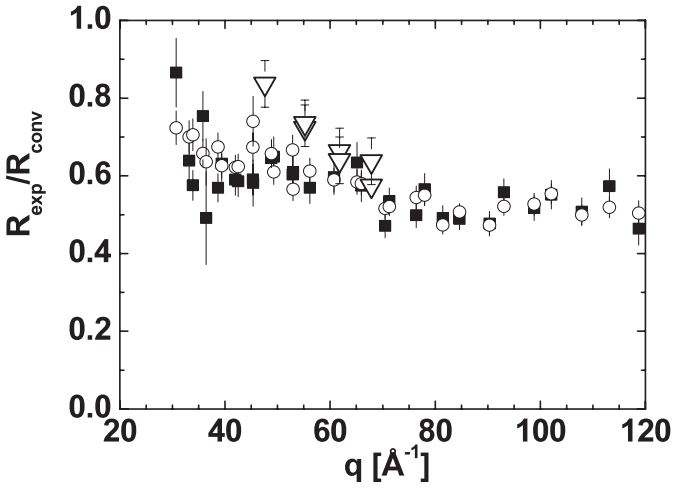

Figure 5. Anomalous reduction of scattering intensity from H of Formvar ($C_8H_{14}O_2$), as a function of momentum transfer q [11]. The results are normalized by dividing the measured cross-section ratios of H to C + O by the 'conventional' ratio 21.6. The full squares represent VESUVIO results for 0:1 mm Formvar foils and the open circles those for 0:2 mm foils. The large open triangles show the results of measurements by high-energy electron–proton scattering from Formvar films of 50–100 Å thickness, as described in [11].

6. The convolution approximation

6.1. Tests using experimental data and DINSMS simulations

The importance of assessing the inaccuracies introduced by the 'convolution approximation' (CA), defined in section 2.3, was discussed by Chatzidimitriou-Dreismann *et al* [3] in the first published measurement of cross-section anomalies on VESUVIO in H_2O/D_2O mixtures. In order to eliminate the possibility that the CA could be responsible for the observed anomalies in this system, two independent checks were made.

(1) A DINSMS simulation of the measurements was made following the procedure outlined in section 4. Although a simulation can never fully reproduce experimental data, it should provide a useful test, since the simulation does not incorporate the CA. An example of a simulation is compared with real data in figure 6 for a 50% mixture of H_2O/D_2O. The ratio σ_H/σ_D, obtained from fitting simulated data, is shown in figure 7, for both Au and U filters, as a function of D concentration x_D. The solid line is the 'conventional' cross-section ratio, input to the simulation. It can be seen that with an Au analyser, the DINSMS simulation predicts that the CA introduces a systematic reduction of the observed ratio σ_H/σ_D by between 5 and 7%. However with a U analyser, fitting simulated data with equation (2.24) recovers the cross-section ratios input to the simulations to within $\sim$1%, over the entire range of concentrations x_D.

(2) The VESUVIO measurement was repeated with a U filter, where the MC simulation indicated that the effects of the CA were negligible. The results of the Au and U filter measurements are also shown in figure 7. It can be seen that the difference between the data with the two filters is consistent with the MC calculation, with an offset of the values obtained from the different filters, but that the slope of the experimental curve is unchanged. Furthermore, the size of the observed anomaly is much larger than the systematic errors introduced by the CA for both Au and U filters.

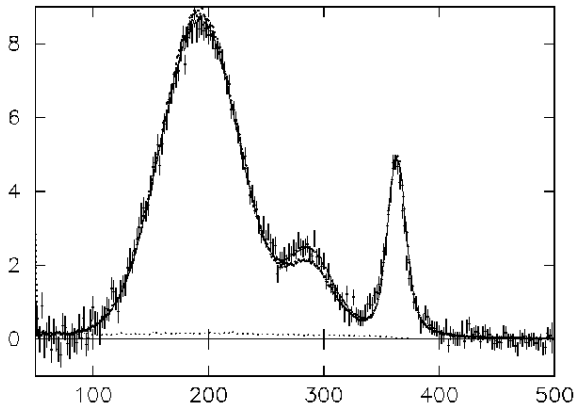

Figure 6. Data (points) and DINSMS simulations for a 0.17 mm thick sample of a 50% mixture of H_2O/D_2O. The solid line was calculated using cross-sections determined from the fitting procedure. The second solid line shows a simulation using the tabulated values for cross-sections and illustrates the larger D cross-section obtained from the data. The dotted line shows the multiple scattering contribution. Three detectors with angles between 58° and 65° were summed to improve the statistical accuracy of the data.

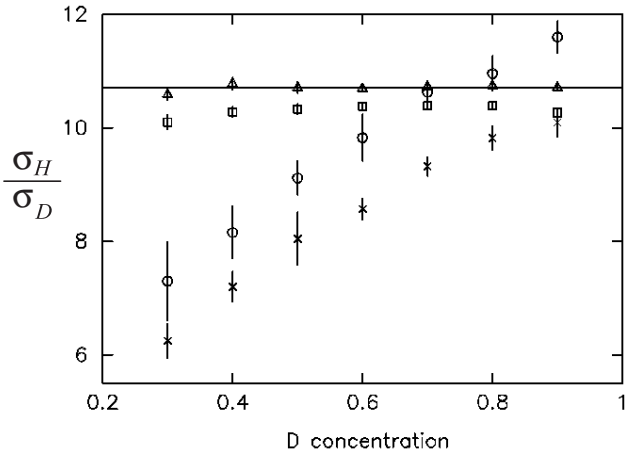

Figure 7. Ratio σ_H/σ_D in H_2O/D_2O mixtures as a function of D_2O concentration. The squares were obtained from an MC simulation with an Au filter. The triangles were obtained from an MC simulation with a U filter. The error bars shown are the standard deviation from the mean over the angular range 50°–75°. The solid line is the ratio 10.7 expected from tabulated values of σ_H and σ_D, input to the MC simulation. The crosses were data [3] taken with an Au filter and the circles data with a U filter.

6.2. Criticisms

It was concluded [3] on the basis of these tests that the CA had no significant effect on the observed anomalous cross-section ratios in H_2O/D_2O mixtures. Simulations of measurements on other systems also indicated that in all cases that the effects of the CA are small and do not significantly affect the results obtained. In contrast to this conclusion Blostein *et al* have produced a series of papers [18–20], arguing that the CA does introduce serious errors into cross-section ratios and that this could explain the anomalies observed in H_2O/D_2O mixtures.

They base this conclusion on their own numerical simulations of the experiments. Their simulations indicate that the systematic errors introduced by the CA are comparable with the observed anomalies, with both Au and U filters. The results in figure 7 should be compared with the calculations of Blostein *et al*, illustrated in figure 4 of [18]. For an Au analyser, we calculate a maximum reduction in σ_H/σ_D of ∼7% at $x_D = 0.3$, compared with the 25% reduction calculated by Blostein *et al*. With a U filter analyser, we calculate a maximum ∼1% reduction in σ_H/σ_D compared with the ∼40% reduction calculated by Blostein *et al*.

One possible explanation of the discrepancy between our calculations and those of Blostein *et al* is that the latter incorporate only the energy resolution, whereas all resolution components are included in the DINSMS simulations. With a U filter, for example, the main resolution component is due to the angular rather than the energy resolution[3]. However, if all resolution widths other than the energy resolution are set to zero in DINSMS, this has little effect on the results obtained from the simulations. The systematic errors in the fit parameters are, somewhat surprisingly, increased by ∼1–2% when other resolution component are neglected, but this cannot explain the large discrepancy between the results of our calculation and those of Blostein *et al*.

The result of Blostein *et al* that the errors introduced by the CA with a U filter are comparable with those introduced with an Au filter are particularly puzzling, and are crucial to their argument that the anomalies are an artefact of the CA. In figure 8(a) we show the filter absorption $A(E_1)$ calculated from tabulated nuclear resonance parameters for Au (solid curve) and U (dotted curve) filters of the thicknesses used in the experiments. Figure 8(b) shows measured data from lead, which is used to determine the energy resolution widths for the two filters [29]. Both calculation and measurements indicate that a factor 2–3 improvement in resolution is obtained with a U filter, compared with an Au filter. A rough estimate of the errors introduced by the instrument resolution function can be obtained by assuming that the intrinsic peak shape in time of flight of width w and the resolution function of width r are both Gaussians. Adding the widths in quadrature thus implies that the measured width w_m is

$$w_m = \left(w^2 + r^2\right)^{1/2} \sim w\left(1 + \frac{r^2}{2w^2}\right). \tag{6.1}$$

With an Au filter, the energy resolution width is typically ∼1/4 that of the intrinsic peak width of H and D peaks, and this introduces a ∼3% increase in the peak width due to resolution effects. With a U filter the resolution width is ∼1/10 that of the peak width and introduces a ∼0.5% increase in peak width. With the assumption that errors introduced by the CA also scale roughly in the same way, one would expect that the effects of the CA would therefore be less by a factor ∼6 with U than Au. This agrees with the factor ∼7 decrease in errors indicated by the MC calculation shown in figure 7. In contrast, Blostein *et al* calculate that the error introduced by the CA for a U filter is almost twice that for an Au filter, despite the much reduced width of the U resolution function, a result which appears to contradict basic physical considerations.

Blostein *et al* have also argued that the large errors they calculate in fitted cross-section ratios are introduced by the wings in the filter absorption $A(E_1)$, which are not properly accounted for by the approximation of the resolution function as a Lorentzian, or by the approximation of incorporating the resolution function as a convolution. However, the wings in the Au resolution function are much more significant than those in the U resolution function. Thus one would expect that if long wings in the resolution function were responsible for the reduced values of σ_H/σ_D, this effect should be larger with an Au filter than a U filter, whereas the Blostein *et al* calculation indicates that it is smaller.

[3] See figure 5(a) of [29].

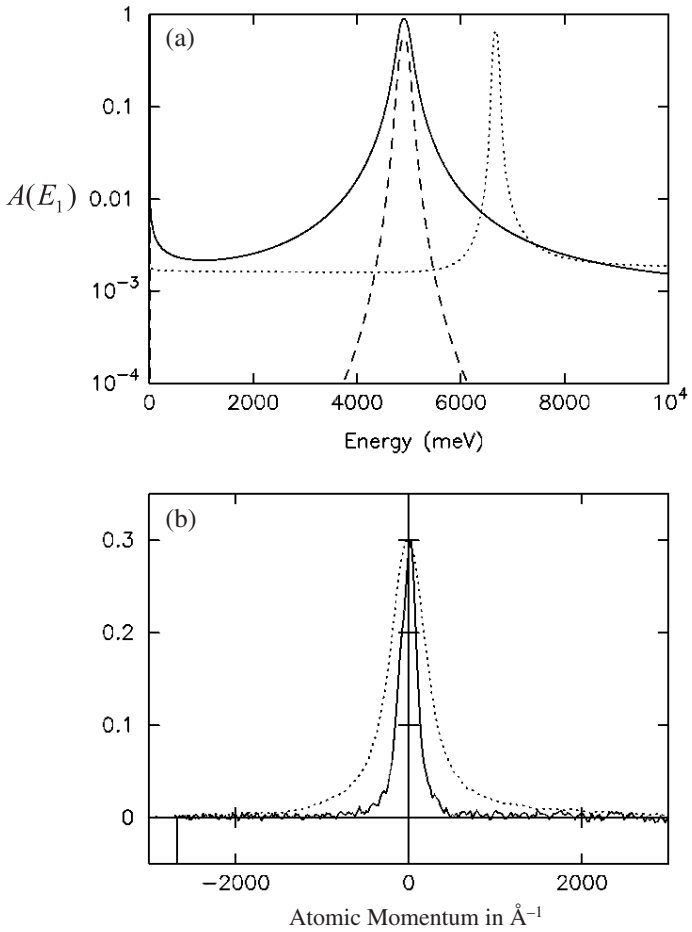

Figure 8. (a) The calculated absorption $A(E_1)$ of the analyser filters as a function of E_1. The solid curve is for the Au filter in single difference. The dotted curve is for the U filter in single difference. The dashed curve is for the Au filter in double difference. (b) Measured data from lead for an Au filter (dotted curve) and for a U filter (solid curve) in momentum space. The measurement is resolution dominated and is used to determine the energy resolution function $D(E_1)$.

6.3. Double difference measurements

A further experimental check on the possibility that long wings in $A(E_1)$ could affect the cross-section ratios derived from fitting has recently become possible with the installation of the 'double difference' (DD) technique [30] on VESUVIO. This consists of taking three measurements: with no filter, with a filter of thickness d_1 and absorption $A_1(E_1)$, and with a filter of thickness d_2 and absorption $A_2(E_1)$. The 'double difference' of the three measurements is

$$R_{\mathrm{DD}}(E_1) = A_1(E_1) - \frac{d_1}{d_2}A_2(E_1). \tag{6.2}$$

The DD technique relies upon the fact that when $\sigma(E)$ is small,

$$A_1(E_1) = 1 - \exp[-Nd_1\sigma(E_1)] \sim Nd_1\sigma(E_1) \tag{6.3}$$

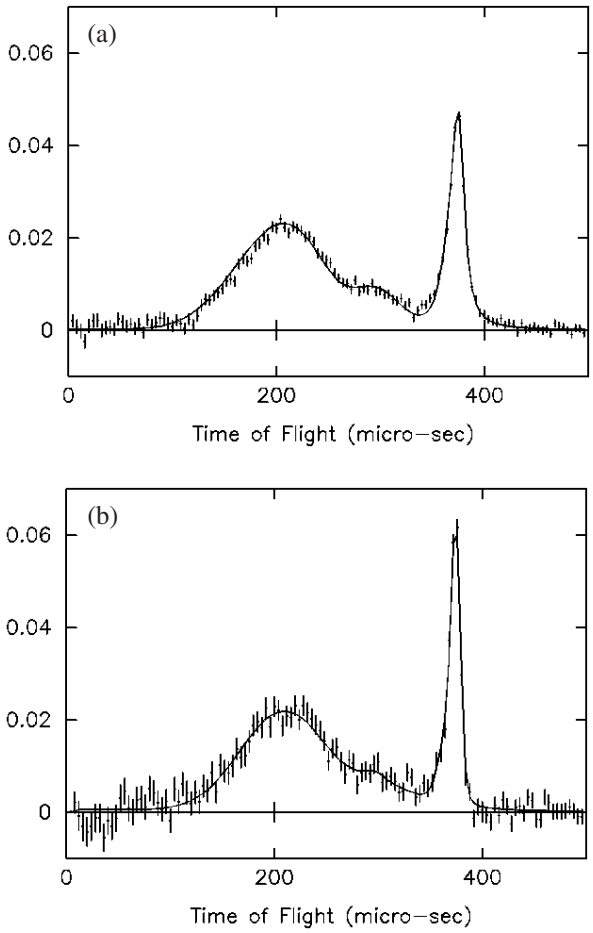

Figure 9. (a) The sum of data and fits from 8 detectors in the angular range 53°–68°, for a 50:50 mixture of H_2O/D_2O, using the single difference technique. (b) The sum of data and fits from the same 8 detectors in the angular range 53°–68°, for a 50:50 mixture of H_2O/D_2O, using the double difference technique.

with a similar expression for $A_2(E_1)$. Thus when $\sigma(E)$ is small $R_{DD}(E) = 0$ and the wings of the function $A_1(E_1)$ in single difference (SD) are removed, whatever their functional form. This is illustrated in figure 8(a), where the calculated energy resolution function $R_{DD}(E_1)$ for an Au analyser is also shown.

Figure 9 shows recent data collected from a 50:50 mixture of H_2O/D_2O using both the SD and DD methods. The improved resolution of the DD data is most obvious in the narrowing of the width of the peak at $\sim$370 μs, which is a combination of scattering from the O atom and the niobium container. The mean of σ_H/σ_D over 16 detectors in the angular range 50°–80° was $8.20 + -0.09$ for the SD data and $7.70 + -0.20$ for the DD data. Both results are in good agreement with the results given in [3] at the same concentration. Figure 10 shows the results of fitting to the SD and DD data for Formvar ($C_8H_{14}O_2$)[4]. Again there is a slight increase in the anomalies when the DD method is used. This is the opposite trend to that which would be expected, if the anomalies were due to the method used to incorporate the resolution function.

[4] Unpublished data from [11].

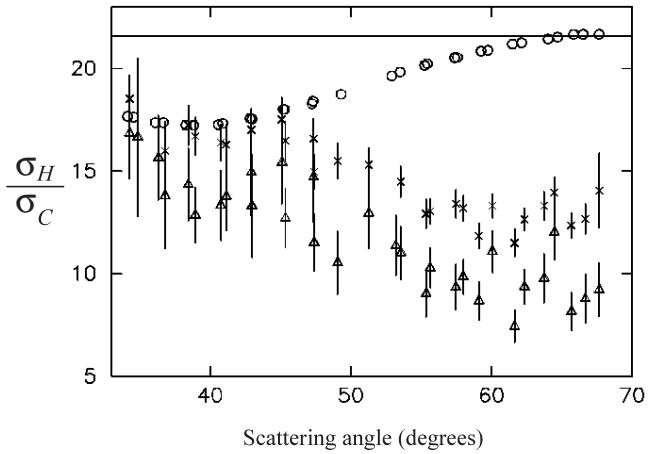

Figure 10. Data for Formvar, [11]. The solid line is the calculated ratio of $H/(C+O) = 21.6$. The crosses are the single difference results and the triangles are the double difference results. The circles were determined from the DINSMS simulation described in section 9.

To summarize, the calculations of Blostein *et al* disagree with our MC simulations. Their results are also counterintuitive, with a factor ∼2 increase in the errors introduced by the CA, when the resolution width is decreased by a factor 2–3. Whereas their simulations have not been tested against real data, it has been shown that DINSMS accurately reproduces both single and multiple scattering in VESUVIO data for atomic masses ranging between 1 and 207 [31]. We also stress that DINSMS incorporates the energy resolution of VESUVIO accurately. To within 1–2%, simulated lead calibration measurements give the same widths for the energy resolution function as real calibrations, for both Au and U filters. The fact that the anomalies observed on VESUVIO are essentially the same for energy resolution functions varying in width by a factor 2–3, whether or not significant wings are present, also provides very strong experimental evidence that the effects of the convolution approximation are small and cannot explain the observed anomalies.

7. Sample size effects

A series of measurements on H_2O/D_2O mixtures with $x_D = 0.5$, listed in table 2, with a variety of sample geometries and scattering intensities varying by a factor ∼5, have given the same ratio σ_H/σ_D, within error. Similarly in NbH [4] and Formvar [11] (see figure 5), varying the sample thickness by a factor two made no difference to the cross-section ratios obtained. The fact that the results are independent of the sample size is very strong evidence that sample attenuation effects and multiple scattering play no significant role in the observed anomalies. Multiple scattering corrections can also be calculated using DINSMS, as described in [31]. This was done for the thickest sample used in the H_2O/D_2O experiments (0.5 mm) and the ratio σ_H/σ_D, obtained from fitting data, with and without a correction for multiple scattering, are shown in figure 11. The form of the multiple scattering contribution is shown in figure 6. It can be seen that calculated multiple scattering effects are essentially negligible.

Another possible cause of the reduction in the intensity of H peaks, observed in data as the scattering angle is increased in NbH [4] and Formvar [11], is the presence of dead time effects in the VESUVIO detectors. This would have the effect of making the detector efficiency $\eta(E_1)$ a function of time of flight t, with lower $\eta(E_1)$ at short t, where the count rate is largest. Since

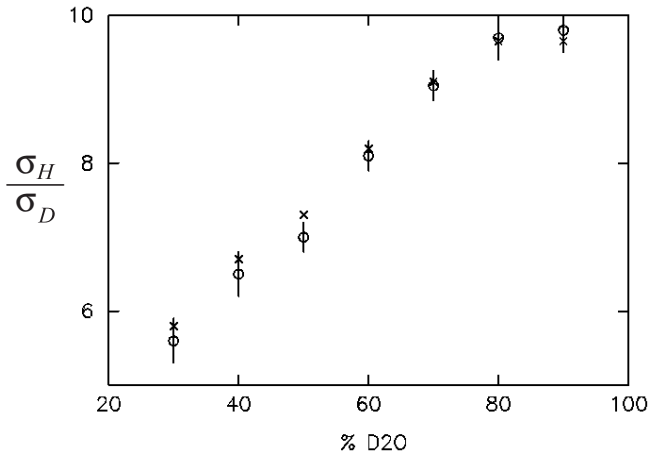

Figure 11. The ratio σ_H/σ_D with (crosses) and without (circles) a correction for multiple scattering, for data taken with an Au analyser filter.

Table 2. The ratio σ_H/σ_D for 50:50 H_2O/D_2O mixtures measured with different materials for the sample can and different scattering geometries and scattering powers. The scattering power was determined by comparing the sample scattering at 60° with that from a 1 mm thick lead sample.

Date	Can material	Geometry	Thickness	Scattering power (%)	σ_H/σ_D
March 1995	Al	Flat	0.5 mm	6.5	8.0 ± 0.5
July 1995	V	Flat	0.2 mm	3.3	7.6 ± 0.2
May 1997	Al	Flat	0.5 mm	15	7.4 ± 0.2
Aug. 1997	V	Flat	0.2 mm	7.5	7.8 ± 0.5
June 1998	Al	Annular	0.5	12	7.5 ± 0.5
June 1998	Nb	Annular	0.5	12	7.0 ± 0.4
Jul. 2003	Nb	Annular	0.5	8.4	8.2 ± 0.1

the H peak moves to lower t as the scattering angle increases, this would introduce a reduction in intensity of the H peak with increasing scattering angle, similar to that observed in Formvar and metal hydride systems. A number of independent checks on the electronic counting chain, detailed in [5], have been made to eliminate this possibility. Most conclusively, the fact that the effects observed on VESUVIO are essentially independent of count rates varying by a factors of up to ∼5 demonstrates that dead time effects have no significant influence on the results.

8. Deviations from the IA

The corrections to the IA for the finite q of measurement, known as 'final state effects' (FSE), have been extensively discussed in the literature [24–28]. The method of [24] is incorporated in standard VESUVIO data analysis routines. He showed that the effects of finite $\vec{q}$ and ω can be accounted for by expressing the neutron Compton profile $J(y)$ as

$$J(y) = J_{\mathrm{IA}}(y) + \frac{M\langle\nabla^2 V\rangle}{36\hbar^2 q}\frac{\mathrm{d}^3 J_{\mathrm{IA}}(y)}{\mathrm{d}y^3} + \frac{M^2\langle F^2\rangle}{72\hbar^4 q^2}\frac{\mathrm{d}^4 J_{\mathrm{IA}}(y)}{\mathrm{d}y^4} + \cdots \tag{8.1}$$

where $J_{\mathrm{IA}}(y)$ is the IA result. $\langle\nabla^2 V\rangle$ is the mean value of the Laplacian of the potential energy of the atom and F is the force on the atom. At the q values observed on VESUVIO, it is only

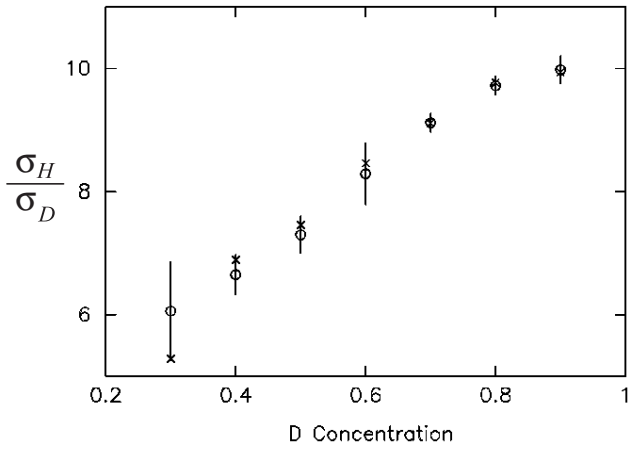

Figure 12. σ_H/σ_D; the circles include a correction for deviations from the IA, while the crosses do not.

necessary to include the first correction term in (8.1) in the analysis. It is assumed that the FSE in H and D atoms are identical to those observed in an isotropic harmonic potential, implying that $\langle \nabla^2 V \rangle = 12\hbar^2 w_M^4/M$, where w_M is the Gaussian width defined in equation (2.25). Within this approximation FSE can be incorporated into the fitting expression for $J_M(y_M)$, without increasing the number of fitting parameters. It has been shown previously [34] that this parameterization of FSE is broadly consistent with deviations from the IA observed on VESUVIO.

The effects of FSE were evaluated by fitting time of flight data from the different mixtures of D_2O and H_2O, described in [3], with and without an FSE correction of the form given in equation (8.1), in the fitting expression. The mean values of σ_H/σ_D over the angular range 50°–75°, obtained by the two procedures, are shown in figure 12. It can be seen that the differences are small and that the trend to smaller values of σ_H/σ_D with decreasing x_D is essentially the same. This indicates that FSE on VESUVIO have little effect on the measured ratio σ_H/σ_D in this system. Similar comments apply to other systems studied.

9. Peak shapes

The approximation that $J(y)$ for all masses is a Gaussian function has also been questioned [16]. Recently it has become possible to fit the peak shapes of VESUVIO data exactly and hence to measure $J(y)$, without any assumptions about the peak shape [35]. In figure 13 we show the $J(y)$ derived for the H atom in Formvar using the procedure given in [35], together with the best Gaussian fit. It can be seen that there are wings in $J(y)$, which are not well described by a Gaussian function. An MC simulation of Formvar data was made with the measured $J(y)$ for H in figure 13, input to the simulation. The C and O peaks were represented as Gaussians. The latter assumption should be a good one since the widths of these peaks are resolution dominated. The results of analysing the simulated data, with the standard fitting programs, assuming Gaussian peak shapes for all atoms are shown in figure 10. It can be seen that the simulation gives an increase in σ_H/σ_C with increasing scattering angle. This can be understood in terms of the decreasing overlap between the H and heavy atom peaks as the scattering angle is increased, and is the opposite trend to that observed in the data. Simulations for NbH [4] gave similar results to those for Formvar with an increase of ∼7% in the ratio σ_H/σ_{Nb} as the

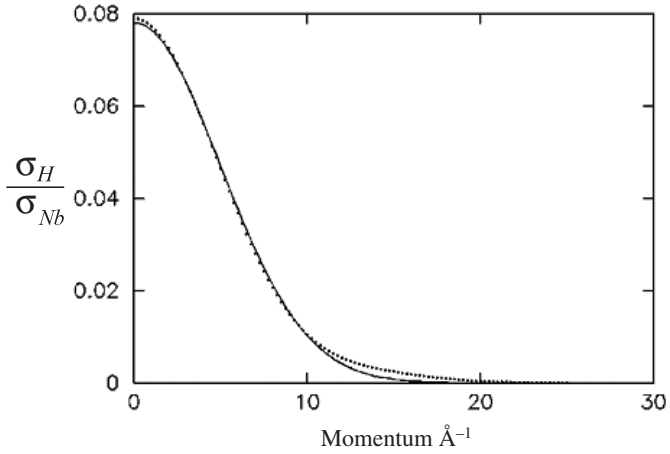

Figure 13. $J(y)$ determined for H in Formvar, using the procedure of [35], as dots. The best Gaussian fit to $J(y)$ is shown as the solid curve.

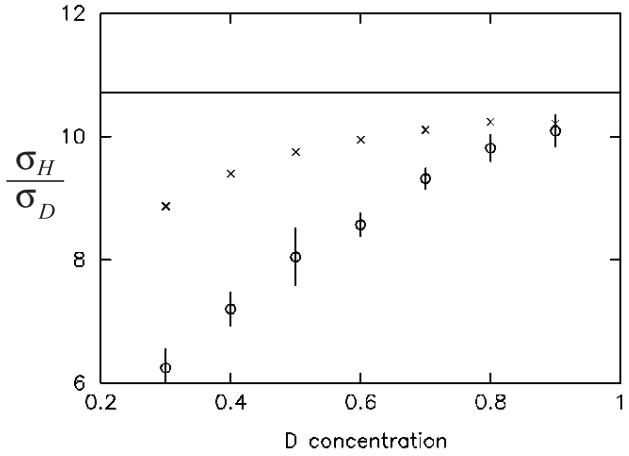

Figure 14. The crosses show σ_H/σ_D obtained by fitting simulated data with non-Gaussian peak shapes for H and D with the standard fitting programs, which assume that the peak shapes are Gaussian. The circles show values of σ_H/σ_D obtained by fitting experimental data.

angle was increased between 30° and 80°, compared with the ∼40% decrease observed in real data. A similar procedure was followed to simulate data for H_2O/D_2O mixtures as a function of x_D, using measured non-Gaussian $J(y)$ for the H and D peak shapes. The results of fitting the simulated data are shown in figure 14. It can be seen that, in this case, the non-Gaussian peak shapes do reduce the fitted ratio σ_H/σ_D, in a similar way to that observed in data, although only by ∼30% of the observed value.

10. Conclusions

We have demonstrated that the following considerations cannot explain the observed cross-section anomalies.

(1) Inaccuracies in the incident intensity, as suggested by Cowley [16]. The Jacobian dE_0/dt is a standard textbook expression [23] and is simply calculated. The incident beam spectrum $I(E_0)$ has been calculated [33] and measured in two different ways, with the same result, within ∼4%, whereas errors in the measured $I(E_0)$ would have to be at least ∼20% to explain the results obtained. The fact that a number of systems give cross-section ratios that are independent of angle also suggests very strongly that the anomalous cross-sections cannot be explained in this way.
(2) The way in which the energy resolution function is incorporated into the data analysis as suggested by Blostein *et al* [18–20]. Since the results are essentially independent of a wide range of different resolution functions, with or without long wings, it is clear that this suggestion cannot account for the anomalies.
(3) Since the results obtained are independent of sample geometry and scattering power, sample attenuation, multiple scattering and detector dead time effects can all be eliminated as a possible cause of the observed anomalies.

The agreement obtained between neutron and electron–proton scattering [11] measurements also provides strong experimental evidence that the three effects above cannot explain the observed anomalies. The remaining assumptions of the analysis, that the scattering can be described within the impulse approximation and that neutron Compton profiles are Gaussian, are shared by the analysis of electron–proton scattering and neutron scattering data and therefore cannot be eliminated quite so conclusively as a possible cause of the observed anomalies. However, simulations using the measured peak shapes indicate that the effect produced by the assumption of Gaussian peak shapes is too small to account for the observations in H_2O/D_2O systems. Furthermore, the trend to lower cross-sections for H with increasing q, observed in NbH and Formvar, is masked rather than enhanced by the effect of peak shapes. Thus we conclude that there is strong evidence that the observed anomalies are due to a breakdown of standard neutron scattering theory at eV energy transfers and are not an artefact of the VESUVIO instrument or the data analysis procedures employed.

References

[1] Chatzidimitriou-Dreismann C A 1991 *Adv. Chem. Phys.* **80** 201
Chatzidimitriou-Dreismann C A 1997 *Adv. Chem. Phys.* **99** 393
[2] Chatzidimitriou-Dreismann C A, Krieger U K, Möller A and Stern M 1995 *Phys. Rev. Lett.* **75** 3008
[3] Chatzidimitriou-Dreismann C A, Abdul Redah T, Streffer R M F and Mayers J 1997 *Phys. Rev. Lett.* **79** 2839
[4] Karlsson E B, Chatzidimitriou-Dreismann C A, Abdul Redah T, Streffer R M F, Hjörvarsson B, Öhrmalm J and Mayers J 1999 *Europhys. Lett.* **46** 617
[5] Karlsson E B, Abdul-Redah T, Streffer R M F, Hjörvarsson B, Mayers J and Chatzidimitriou-Dreismann C A 2003 *Phys. Rev.* B **67** 184108
[6] Abdul-Redah T, Streffer R M F, Chatzidimitriou-Dreismann C A, Hjörvarsson B, Karlsson E B and Mayers J 2000 *Physica* B **276–278** 824
[7] Chatzidimitriou-Dreismann C A, Abdul Redah T and Sperling J 2000 *J. Chem. Phys.* **113** 2784
[8] Chatzidimitriou-Dreismann C A, Abdul Redah T, Streffer R M F and Mayers J 2002 *J. Chem. Phys.* **116** 1511
[9] Chatzidimitriou-Dreismann C A, Abdul-Redah T and Kolaric B 2001 *J. Am. Chem. Soc.* **123** 11945
[10] Abdul-Redah T and Chatzidimitriou-Dreismann C A 2003 *J. Alloys Compounds* **356** 249
[11] Chatzidimitriou-Dreismann C A, Vos M, Kleiner C and Abdul-Redah T 2003 *Phys. Rev. Lett.* **91** 57403
[12] Chatzidimitriou-Dreismann C A 2003 *J. Alloys Compounds* **356/357C** 244
[13] Karlsson E B and Lovesey S W 2000 *Phys. Rev.* A **61** 62174
[14] Karlsson E B and Lovesey S W 2002 *Phys. Scr.* **65** 112
[15] Karlsson E B 2003 *Phys. Rev. Lett.* **90** 95301
[16] Cowley R A 2003 *J. Phys.: Condens. Matter* **15** 4143
[17] Colognesi D 2004 *Physica* B **344** 73–81
[18] Blostein J J, Dawidowski J and Granada J R 2001 *Physica* B **304** 357

[19] Blostein J J, Dawidowski J and Granada J R 2003 *Physica* B **334** 257
[20] Blostein J J, Dawidowski J, Ibàńez S A and Granada J R 2003 *Phys. Rev. Lett.* **90** 105302
[21] Blostein J J, Dawidowski J and Granada J R 2004 *Nucl. Instrum. Methods* B **217** 333–341
[22] Lovesey S W 1984 *Theory of Neutron Scattering from Condensed Matter* vol 1 (New York: Oxford University Press)
[23] Windsor C 1981 *Pulsed Neutron Scattering* (London: Taylor and Francis) equation (9.30)
[24] Sears V F 1984 *Phys. Rev.* B **30** 44
[25] Mayers J, Andreani C and Baciocco G 1989 *Phys. Rev.* B **39** 2022
[26] Mayers J 1990 *Phys. Rev.* B **41** 41
[27] See Glyde H R 1994 *Phys. Rev.* B **50** 6726 for a recent review of the literature on FSE
[28] Evans A C, Timms D N, Mayers J and Bennington S 1996 *Phys. Rev.* B **53** 3023
[29] Fielding A L and Mayers J 2002 *Nucl. Instrum. Methods* A **480** 680
[30] Seeger P A, Taylor A D and Brugger R M 1985 *Nucl. Instrum. Methods* A **240** 98
[31] Mayers J, Fielding A L and Senesi R 2002 *Nucl. Instrum. Methods* A **481** 454
[32] Mughabgab S F 1984 *Neutron Cross Sections* (Orlando, FL: Academic)
[33] Taylor A D 1984 *Rutherford Appleton Laboratory Report* RAL-84-120
[34] Evans A C, Timms D N, Mayers J and Bennington S 1996 *Phys. Rev.* B **53** 3023
[35] Reiter G F, Mayers J and Noreland J 2002 *Phys. Rev.* B **65** 104305